Models for biomedical interfaces: a computational study of quinone-functionalized amorphous silica surface features

Models for biomedical interfaces: computational study of quinone-functionalized amorphous silica surface features†

Marta Corno[1,], Massimo Delle Piane[2], Patrick Choquet[3] and Piero Ugliengo[1]*

[1]Dipartimento di Chimica and NIS – Nanostructured Interfaces and Surfaces – Centre, Università degli Studi di Torino, via P. Giuria 7, 10125, Torino, Italy

[2]Faculty of Production Engineering and Bremen Center for Computational Materials Science, University of Bremen, Am Fallturm 1, 28359, Bremen, Germany

[3]Luxembourg Institute of Science and Technology (LIST), Materials Research and Technology Department (MRT), 5, avenue des Hauts-Fourneaux, L-4362 Esch/Alzette, Luxembourg

*Corresponding author: marta.corno@unito.it, telephone: +390116704597

Keywords. DFT methods; Ab-initio; silica surfaces; functionalization; quinone; catechol; Ab-Initio-Molecular-Dynamics simulations; CRYSTAL code; CP2K; biomaterial interfaces.

Abstract

A Density Functional Theory (PBE functional) investigation is carried out, in which a model of amorphous silica surface is functionalized by ortho-benzoquinone. Surface functionalization with catechol and quinone-based compounds is relevant in biomedical fields, from prosthetic implants to dentistry, to develop multifunctional coatings with antimicrobial properties. The present study provides atomistic information on the specific interactions between the functionalizing agent and the silanol groups at the silica surface. The distinct configurations of the functional groups, the hydrogen bond pattern, the role of dispersion forces and the simulated IR spectra provide a detailed insight on the features of this model surface coating. *Ab-initio* molecular dynamics gives further insights on the mobility of the functionalizing groups. As a final step, we studied the condensation reaction with allylamine, via Schiff base formation, to ground subsequent simulations on the condensation with model peptides of antimicrobial activity.

Introduction

Biomaterials are among the most widely studied materials in the last decades. Life expectancy has increased, thus strongly requiring the production of engineered materials capable to integrate and dynamically interact within the aged or damaged tissues of human body. In dentistry, the focus is to design materials with antimicrobial properties against bacterial infections in surgery, eventually leading the failure of the dental implant.[1] This issue, named "the race for the surface" by Anthony G. Gristina in 1987,[2,3] causes both economic and societal problems and has become a scientific challenge, involving different disciplines, such as chemistry, physics, medicine, material science and engineer. Designing specific interfaces on the biomaterials without using toxic substances or promoting bacterial resistance still represents a critical task.

To this aim, antimicrobial peptides (AMPs) represent one of the best solutions, being active biomolecules produced by a wide variety of organisms (plants, mammals, insects, marine invertebrates, ...) as an essential component of their innate immune response.[4] Within the dentistry research area,[5] AMPs have been studied against bacteria growing in the oral cavity and as dental-caries preventing agents. The activity of the immobilized AMPs strongly depends on the length and kind of spacer between the active biomolecules and the solid matrices. Therefore, the search for a specific linker, i.e. a bio-inspired organic precursor, for the adhesion of the AMPs to the engineered biomaterial surface has led to different candidates. Among many, 3,4-dihydroxy-L-phenylalanine (DOPA) is a crucial species for conferring the peculiar adhesive properties to marine mussels. For instance, the comprehension of collagen and adhesive mussel foot proteins (mfps) interactions can generate improved medical and dental adhesives, particularly for collagen-rich tissues.[6] Examples of applications of these molecules include the design of cell and protein resistant surfaces desired for implantable medical implants and diagnostics as well as for antiicing coatings on aircraft wings and nonfouling marine surfaces.[7]

Catechol and benzoquinone molecules have become relevant in studying protein surface adhesion as

versatile building blocks for designing mussel-inspired coatings,[8,9] since catechols - benzene derivatives with two neighboring (ortho-) hydroxyl groups – are easily oxidized to the corresponding DOPA-quinone. The latter can act as a covalent cross-linking unit, either by reacting with nucleophilic groups in the polypeptidic matrix by means of Michael-type additions, or via direct free-radical arylaryl couplings.[10] In a recent study dealing with these moieties, Lee et al. have reported the use of catechol-functionalized polymers as dental adhesives to reduce the failure of dental implants.[11]

Different techniques can be applied for synthetizing the inorganic surface to which the linker and the antibacterial peptide are attached. Among these, the atmospheric pressure Dielectric Barrier Discharge (AP-DBD) plasma polymerization process represents a versatile mass production technique and a green process compared to traditional wet chemical approaches. It has been already successfully used for the elaboration of anti-bacterial surfaces.[12–14] When vinyltrimethoxysilane (VTMOS) is utilized for plasma deposition on the metallic surface, a silica thin film is formed. Such two-dimensional (2D) silica films are relevant also in several other applications, such as dielectric layers in integrated circuits and supporting substrates for catalysis.[15] Recently, some of us have shown that quinone functionalized hybrid layers deposited on stainless steel can be exploited for enzyme grafting, in order to depollute water by degrading amoxicillin, a commonly used antibiotic.[16] Catechols are also used for trapping radicals or metal ions.[17] The reaction of the quinone groups with the amine, thiol and/or imidazole groups of a specific enzyme follows a Michael type addition or with a Schiff base formation (for amine groups) in mild pH condition.[9]

In recent years, computational methods have become a powerful complementary or even alternative tool for the investigation of these functional inorganic-bioorganic interfaces. A recent review gives an overview of the different computational methods both at the smaller length scale of quantum mechanics and at the larger of coarse grain.[18] A large number of computational studies dealing with amorphous silica interface with water and peptides can be found in the literature.[19–21] Specifically, for antimicrobial

peptides, computational studies can help clarifying the mechanism of action, which is still poorly understood. For instance, Cirac et al.[22] adopted a combination of molecular dynamics and experimental investigations to study a family of pore forming cyclic antimicrobial peptides.

Recently, the interaction among catechol moieties and inorganic oxides has been studied by ab-initio molecular dynamics calculations for the adsorption of catechol on a wet TiO_2 (110) interface.[23] Catechol on wet silica surface was computed within DFT and MD to elucidate the competition among water and the organic functionality adopted by marine mussel proteins to adhere permanently to diverse wet surfaces.[24] The main conclusion was that catechol makes a direct contact with the silica surface, displacing water molecules. The same group also confirmed these results recently.[25]

Quinones are also relevant as cofactors for proteins in bioenergetic cycles. In that respect, DFT calculations of EPR/ENDOR parameters confirmed the essential role of hydrogen bonding formation of both neutral and radical anion ubiquinone species with bacterial centers of the specific photosynthetic purple bacterium called *Rhodobacter (Rb.) sphaeroides*.[26]

Moreover, a recent work by Yeh et al. revealed a stronger interaction of catechol molecule compared with the phenolic moieties, on hydroxylated alumina surface in aqueous conditions. The key point was the strong cooperative hydrogen bonding interactions of two neighboring hydroxyl groups with the surface hydroxyl groups of alumina.[27]

To date, understanding the elemental behavior and assembly of catechols on surfaces still remains a challenge. To gain more insight into this issue, Ruiz-Molina et al. studied the self-assembly and interaction of long-chain alkylcatechols with surfaces by means of experimental techniques and molecular dynamics calculations.[28]

In this paper, we studied at the DFT-PBE level of theory, models of ortho-benzoquinone functionalization on amorphous silica surfaces, as a preliminary step for condensation of biomolecules, such as antimicrobial peptides. We have applied here the same computational approach already

successfully adopted on cristobalite surfaces, to study acidic and basic functionalizations.[29] We show that these models are useful also for modeling reaction with a -NH_2 aminoacidic residue of a protein becoming attached to the functionalized surface. To this purpose, we have considered allylamine, but our results can be extended to more complex biomolecules, sporting the same –NH_2 group. The benefit of our computational approach is to provide atomistic models of such a complex interface like a silica catechol-functionalized surfaces and to support spectroscopy experiments by predicting vibrational adsorption in the C=O fingerprint region.

Computational details

Static calculations

For all the static calculations, we adopted the Density Functional Theory framework with the General Gradient Approximation-Perdew-Burke-Ernzerhof (DFT-GGA-PBE)[30] with Grimme's D2 dispersion[31] as encoded in the periodic CYSTAL14 code.[32] We referred to the same split-valence double- and triple-ζ basis set plus polarization functions[33,34] employed in ref. 45. This choice was originally aimed at reducing the basis set super-position error (BSSE), and have proven as a very good compromise also here. Different basis sets were employed to describe the atoms of the silica surface and those of the functionalizing groups, balancing precision and computational cost of the calculations. For more details on the basis set, please refer to the Electronic Supporting Information (ESI). The Hamiltonian matrix was diagonalized in Γ point (shrinking factor IS=1) due to the large size of the surface unit cells. We adopted default values for the tolerances controlling the accuracy of the Coulomb and exchange series (see ESI for details). A true slab model, periodic only in 2 dimensions, was simulated by applying periodic boundary conditions, and the atomic coordinates of the two more exposed atomic layers, reported in the ESI, were optimized *via* an analytical gradient method, upgrading the numerical Hessian with the Broyden-Fletcher-Goldfarb-Shanno algorithm. The other atoms and the unit cell parameters

were kept fixed for all the models at the optimized values for the free silica surface, to compensate for the limited thickness of the slab model. All graphical inspections were carried out with the molecular graphics program MOLDRAW.[35]

We computed the PBE-D2 vibrational frequencies only on a fragment of the slab model, consisting of all silanol OHs and the functionalizing groups, within the harmonic approximation, by obtaining the eigenvalues from the diagonalization of the mass-weighted Hessian matrix. The second derivatives, needed to build the Hessian matrix, were computed from the analytical gradient by a single displacement (0.003 Å) for each atomic Cartesian coordinate with respect to the equilibrium configuration.[36,37] The Berry phase approach allowed the calculation of the infrared intensity of each normal mode.[38]

The majority of the calculations were performed with the massively parallel version of the CRYSTAL14 code (MPP) run on 32 cores, as average.[39]

Ab initio Molecular Dynamics Simulations

Explorative *ab initio* molecular dynamics calculations were performed using the CP2K code.[40] The Quickstep technique[41] with a mixed plane wave and Gaussian basis set methodology (Gaussian and Plane Wave method, GPW) was employed to calculate the electronic structure. We used the PBE functional, with the Goedecker−Teter−Hutter pseudopotentials[42] triple-ζ basis set with polarization functions (TZVP)[43] augmented with the empirical Grimme's D2 correction.[31] The cutoff for the plane wave basis was set to 400 Ry. AIMD simulations were run at 450 K in the NVT ensemble using the Canonical Sampling through Velocity Rescaling (CSVR) thermostat.[44] The adoption of a relatively high temperature compared to the room temperature was to ensure a good configurational sampling of the potential energy surface experienced by the complex catechol substituent in a relatively short time window. We set up a time step of 0.5 fs, running the dynamics for at least 10 ps (thermostat time constant: 50 fs). Since CP2K requires 3D periodic systems, a value of c = 35 Å was chosen to separate the slab

replicas with enough vacuum. In all cases, and in accordance with the static simulations, we allowed only the superficial layer of the silica slab and the drug molecules to move during the MD simulation. Root Mean Square Deviations along the trajectories were computed only for the 16 atoms of the quinone functionalities.

Results and discussion

Quinone functionalization of the silica surface

The plain amorphous silica model

The adopted amorphous silica surface is a well-established 2D model (slab thickness of 7.2 Å, unit cell composition $H_{22}O_{63}Si_{26}$ and unit cell parameters: a = 12.60 Å, b = 12.83 Å, $\alpha = \beta = 90.0°$ $\gamma = 83.1°$) obtained in our laboratory and validated against several physicochemical properties, including adsorption of different molecules, from small organic acids to larger drugs.[45–47] This model is characterized by a silanol density ρ=4.5 OH·nm^{-2}, close to the experimentally value, measured for fully hydroxylated surfaces (4.9 OH·nm^{-2}).[48] This density corresponds to 8 SiOH surface groups per unit cell, all, in principle, available for the functionalization.

It is recognized that the hydrogen bond pattern between silanol groups plays a key role in determining the strength of silica interaction with adsorbed molecules.[49,50] We suggest that the same role is played in determining the relative stability of a given functionalized surface.

Figure 1 shows the top a) and side b) views of the silica model. Four hydrogen bonds are present at the top surface: two of them are part of a small chain, connecting H, G and F silanols exhibiting the strongest hydrogen bond (G⋯H, 1.81 Å), in line with the well-known correlation between H-bond strength and length.[51] The other two hydrogen bonds are isolated, connecting A to B and D to E silanols, with an average length of 2.0 Å. As shown in Figure 1b), the silanol labelled as A is buried below the average

SiOH plane at the silica surface, so it was not considered as accessible for the functionalization.

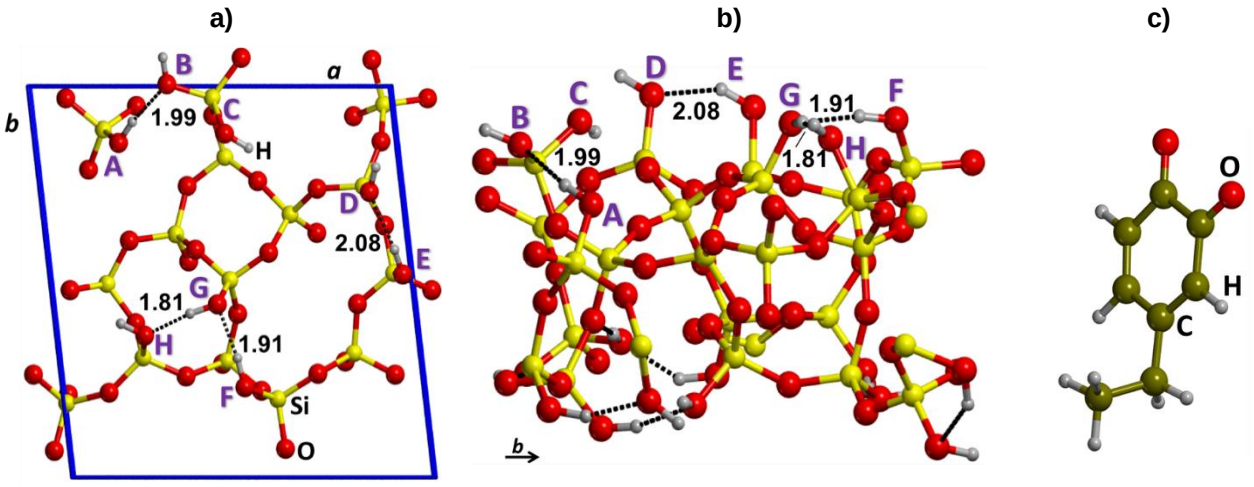

Figure 1. Amorphous silica surface model ($H_{22}O_{63}Si_{26}$, *a* = 12.60 Å, *b* = 12.83 Å, α = β = 90.0° γ = 83.1°) used as a reference for the functionalization: a) top and b) side (along the *b* lattice parameter) views, respectively; unit cell borders in blue; SiOH groups labelled from A to H for future reference; hydrogen bonds represented as black dotted lines, with their length reported in Å; c) 4-ethyl-ortho-benzoquinone or 4-ethyl-1,2-benzoquinone, the reference molecule for the functionalization process. Color code for atoms: silicon in yellow, oxygen in red, hydrogen in light grey, carbon in green.

The chosen reference molecule for the subsequent functionalization reaction (see equation (1)) is the 4-ethyl-ortho-quinone (Figure 1c); the gas phase optimized geometry of the lowest energy conformer was used as a reference energy (see equation 1).

Geometry and energetics of the quinone functionalized silica models

Our chosen computational strategy was to design a number of functionalized structures, by condensation of 4-ethyl-o-benzoquinone on the available silanol groups of the amorphous silica surface model shown in Figure 1 a) and b), as a way of sampling the possible configurations of a functionalized surface. To refer to these models we adopted the same label of the substituted silanols, from B to H (see Figure 1). As abovementioned, silanol A is excluded because not accessible to the incoming molecules. The functionalization process is schematically reported in Figure 2a), while Figure 2b) illustrates, for the specific case involving silanol C, the reference reaction for computing the stability ranking of the seven

structures.

We considered the following reaction as a purely hypothetical one:

$$\text{Silica(OH)}_m + n\text{CH}_3\text{CH}_2\text{-quinone} \rightarrow \text{Silica(OH)}_{m-n}(\text{CH}_2\text{CH}_2\text{-quinone})_n + n\text{H}_2\text{O} \quad (1)$$

as it only serves for calculating relative stability among the possible functionalized surface models rather than mimic any specific experimental reaction. This choice is in agreement with our previous work dealing with the acidic and basic functionalization of the (101) cristobalite surface.[29] In equation (1), *n* is the functionalization degree and its value can be 1 (Figure 3), 2 (Figure 4a) and 3 (Figure 4 b). When we compute the reaction energy ΔE, we separated the electronic contribution coming from the sole PBE energy from that due to the D2 term. In this way, we roughly estimate the relevance of the London energy contribution for each functionalized model, as this has proven crucial in describing the adsorption of aromatic molecules on silica surfaces.[45,47]

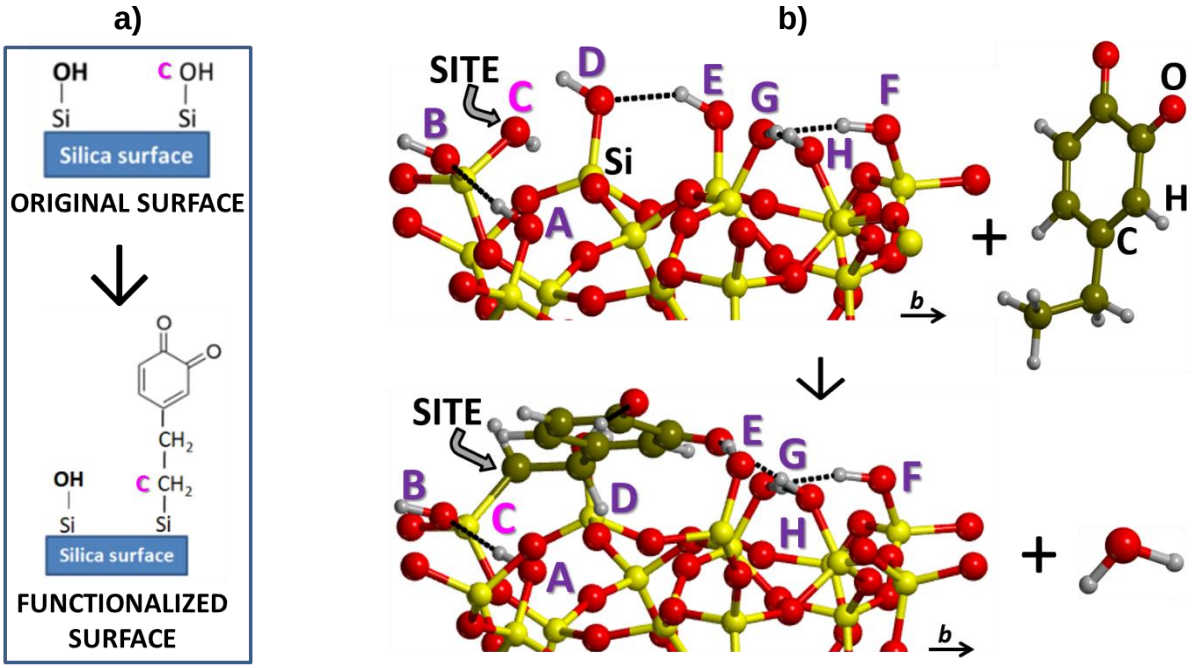

Figure 2. Schematic representation of the reference reaction for the design of functionalized silica surface models, by condensation of 4-ethyl-ortho-benzoquinone on the SiOH group, with the release of a water molecule. a) scheme of the reaction site; b) side views of the chosen amorphous silica surface with the indication of the functionalization site, before and after the reaction (see equation 1), only the two topmost layers are shown. The case of C silanol is chosen as an example. Color code for atoms: silicon in yellow, oxygen in red, hydrogen in

light grey, carbon in green.

We manually docked the functional group of each structure to maximize the number of hydrogen bonds between surface silanols and the C=O groups of the quinone group. Each C=O group can, in principle, establish two hydrogen bonds, for a total number of four hydrogen bonds *per* quinone. The initial guess is then fully relaxed to get the lowest minimum energy structure on the potential energy surface (PES). This approach is nontrivial, since the PES of the system is extremely complex and the manual condensation could easily overlook important interactions and/or the optimization procedure could be stuck in saddle points, at higher energy than the nearest minima. As a practical example of our procedure, we illustrate the case of the B mono-functionalization, Figure 3a) and b). This is a particularly interesting example showing how the hydrogen bond formation influences the stability of the functionalized surface. We started with the optimum model shown in Figure 3a.

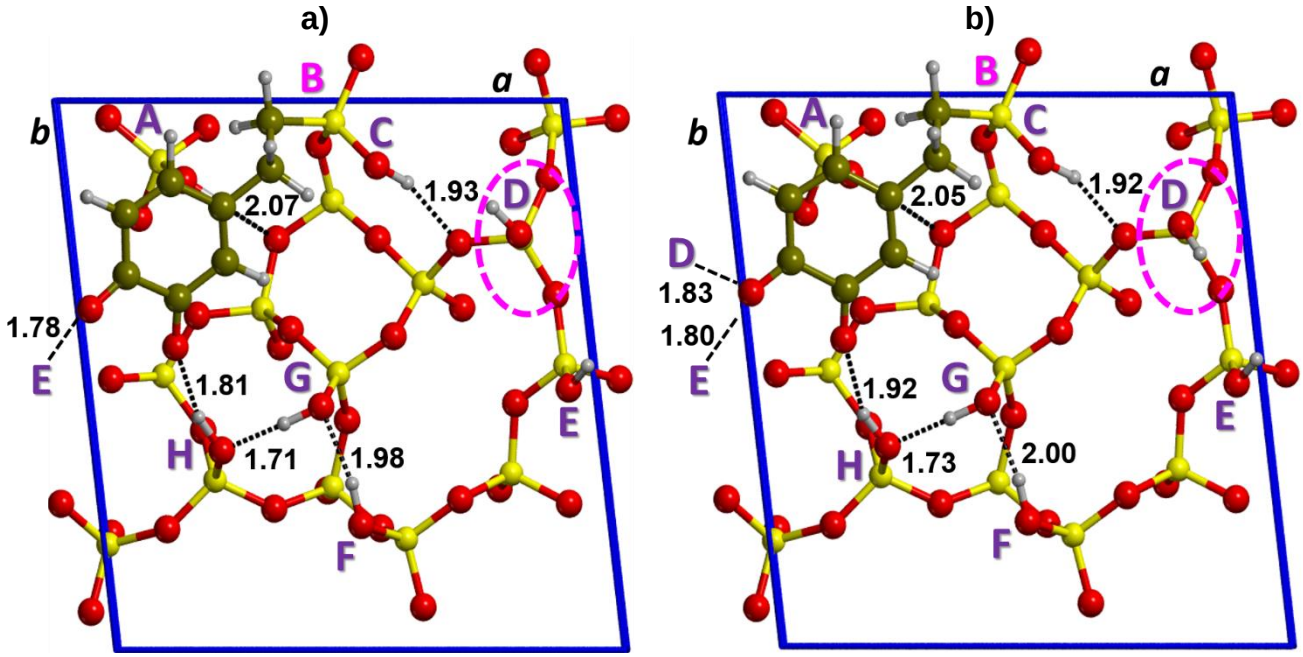

Figure 3. Top views of the unit cell for the case of B-functionalized amorphous silica surface modeling: a) a saddle point on the PES due to SiOH(D) imaginary mode; b) a minimum structure, after rotating silanol D to give a new hydrogen bond with the quinone CO. Color code for atoms: Si in yellow, O in red, H in light grey, C in green; unit cell borders in blue.

This model seems adequate in terms of hydrogen bonds, since each oxygen of the quinone carbonyl group is involved in at least one hydrogen bond of medium strength with a surface silanol. One hydrogen bond involves the E silanol of the nearby unit cell (1.78 Å) and the other silanol H (1.71 Å), which in turn is part of a hydrogen bond chain with G and F silanol groups. From this analysis, structure 3a) appears quite stable as for hydrogen bond interactions. This is confirmed as the computed ΔE= 30.5 $kJ \cdot mol^{-1}$ value is lower than the other cases reported in Table 1 (datum not reported in Table 1, *vide infra*). Nonetheless, when computing the harmonic frequencies (see next section for further details), the structure resulted to be a saddle point and not a minimum in the PES. Graphical inspection of the associated eigenvector has allowed us to arrive to the new model of Figure 3b). In essence, silanol D was rotated to establish a hydrogen bond with the closest oxygen of the quinone functionality. Thus, all seven surface SiOHs participate in a hydrogen bond and the ΔE value lowered to 11.9 $kJ \cdot mol^{-1}$ (see Table 1). As expected, all frequencies were positive for the 3b) model. The dispersive contribution to energy for the two structures (*vide supra*) is higher for the second case (Figure 3b) by only 3 $kJ \cdot mol^{-1}$, which emphasizes a major role of the new hydrogen bond in stabilizing model 3b). This example confirms that extreme care must be taken when applying such a manual static approach for systems with complex PES and that, when possible, a vibrational analysis should be always performed to validate the results.

The same procedure has been adopted for the other six mono-functionalized cases, (C to H ones) and the corresponding optimized structures are reported in Figure 4. Focusing on hydrogen bond patterns, it is evident that the C model is the only case where one C=O group is engaged in two hydrogen bonds with surface silanols E and H, while the other C=O interacts with silanol D (average distance of 1.8 Å). Moreover, the original hydrogen bond pattern H-G-F is retained, with the reinforcement of the hydrogen bond H-G than for the clean surface (1.68 *vs* 1.81 Å). These features confer the C model the highest stability, as reported in Table 1. The B case (see Figure 3b) is characterized by a much higher ΔE=27.8 $kJ \cdot mol^{-1}$ (Table 1) compared to the C case, despite the C=O groups being engaged in three hydrogen

bonds of similar strength (B/C hydrogen bond length: 1.83/1.76, 1.80/1.86, 1.92/1.79, 1.73/1.68, 2.00/1.91, see Figure 3 and 4); as data in Table 1 shows, the difference in the dispersive contribution ΔE_D favors the C model by about 18 kJ·mol^{-1}.

As a counterproof of the synergic role of hydrogen bonds and dispersion in determining the relative stability of a functionalized configuration, a model can be built trying to deliberately reduce these interactions: the resulting G structure is indeed the least stable one, being higher in reaction energy by about 125 kJ·mol^{-1} with respect to the C model. Figure 4 shows that this is the case where the dispersion contribution is at its minimum, as the carbon ring is almost perpendicular to the silica surface. Indeed, the ΔE_D term is 47 kJ·mol^{-1} higher with respect to the C case. Moreover, no hydrogen bonds are formed with the quinone moiety, while the pristine F-G-H hydrogen bond chain at the free silica surface is disrupted.

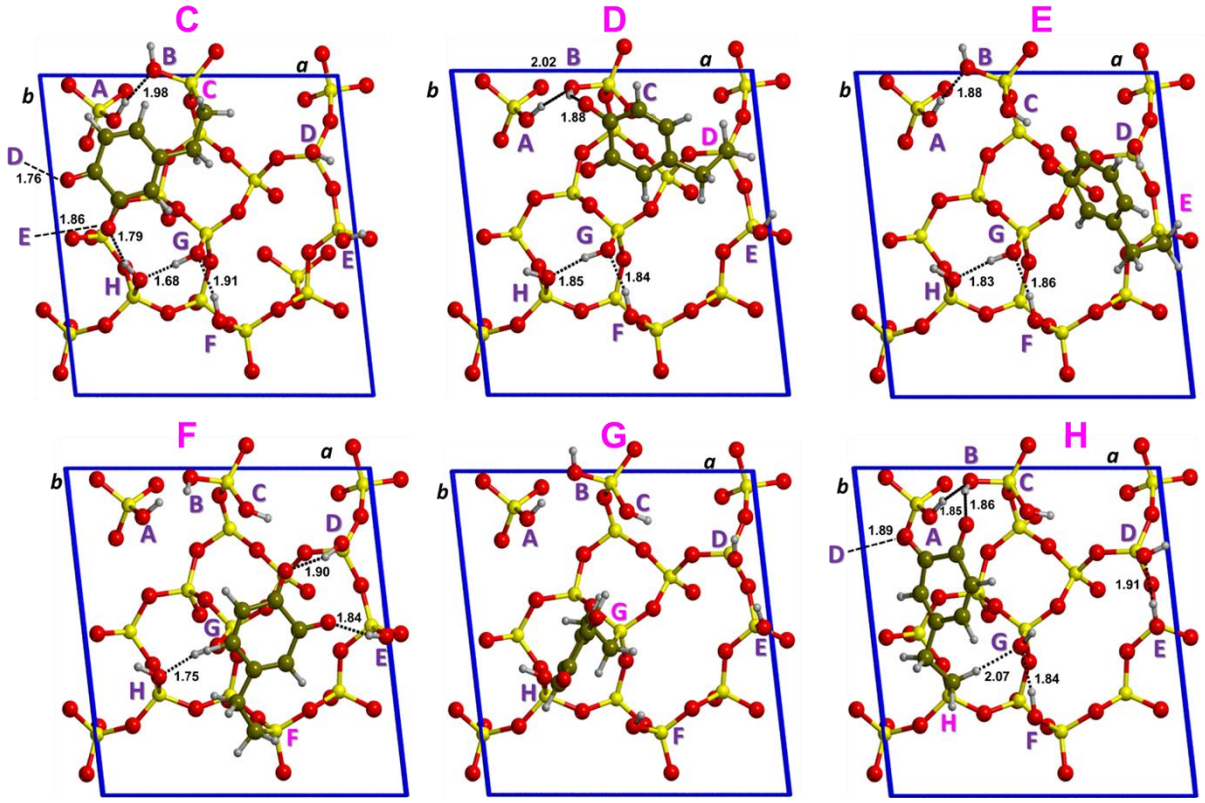

Figure 4. Top views of the six mono-functionalized silica surface models, from C to H case (for the B case see

Figure 3). hydrogen bond represented with black dotted lines and their distances reported in Å. Color code for atoms: silicon in yellow, oxygen in red, hydrogen in light grey, carbon in green.

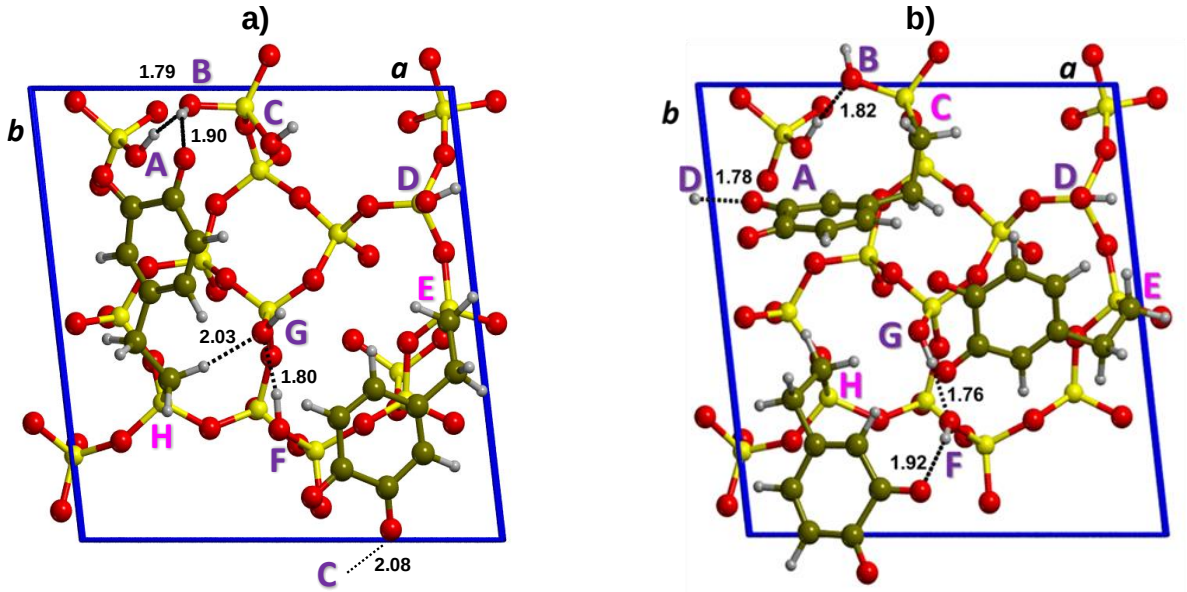

Figure 5. Top views of the two multi-functionalized silica surface models: a) bi-functionalized, with quinone attached to E and H silanols; b) tri-functionalized with quinone attached to C, E and H silanols. hydrogen bond distances reported in Å. Color code for atoms: silicon in yellow, oxygen in red, hydrogen in light grey, carbon in green.

Table 1. Computed reaction energy values (ΔE) for reaction (1), relative stability differences (ΔΔE) with respect to the C model, electronic reaction energy (ΔE_E) and dispersive reaction energy (ΔE_D) for all the considered functionalized models. See Figure 1a) and b) for labelling. Three degrees of functionalization are shown as n=1, 2, 3. All values expressed in kJ·mol^{-1} And expressed per unit of substitution.

	n=1							*n=2*	*n=3*
	B	**C**	**D**	**E**	**F**	**G**	**H**	**HE**	**CHE**
ΔE	11.9	-16.0	43.0	61.6	66.6	108.9	56.7	69.8	43.1
ΔΔE	27.8	0.0	58.9	77.5	82.5	124.9	72.6	85.8	59.1
ΔE_E	65.0	54.8	88.2	116.1	109.5	132.4	125.7	141.9	112.1
ΔE_D	-53.1	-70.7	-45.2	-54.5	-42.9	-23.5	-69.0	-72.1	-69.0

As anticipated, Table 1 reports the reaction energy ΔE for equation (1) and the relative stability ΔΔE of the functionalization product with respect to the most stable C case. The last two columns contain data for models with a higher degree of functionalization, *i.e.* two and three quinone groups per unit cell (see Figure 5 for the corresponding optimized structures). It is worth noting that for the tri-functionalized model, which represents the maximum loading of the original unit cell, the reaction energy, averaged by the number of substituents, is in line with that from mono-functionalized models such as D (see model

CHE in Table 1). This is somehow surprising, as in model CHE one of the quinone groups (the C one, see Figure 5b) does not form neither hydrogen bonds nor significant dispersive interactions with the surface, being almost perpendicular to the surface plane. Clearly, the stabilizing effect due to the other two quinone groups H and E is able to compensate for these lacks of interactions.

Table 1 also shows the relative role played by electronic and dispersive forces, in stabilizing the structures. Interestingly, no general trend can be noticed as regard the relative contributions of ΔE_E and ΔE_D to the total ΔE. However, the most stable C case has the largest negative ΔE_D value, while the least stable model G, the lowest. For B and E models, the ΔE_D values are very close to each other (-53.1/-54.5 kJ mol^{-1}), while ΔE_E favors the B structure by about 50 kJ mol^{-1}. Moreover, for the H model the ΔE_D term is as large as that for the most stable C structure. Dispersive forces are, by definition, always attractive and, being less dependent on the relative orientations, show a limited variability among the different mono-functionalized models (standard deviation = 16.3 kJ mol^{-1}), with respect to the electronic contributions (standard deviation = 30.2 kJ mol^{-1}) that are much more responsive to variation in the geometries of the hydrogen bond interactions.

Computed IR frequencies of quinone functionalized silica models

IR spectroscopy may reveal the effect of the chemical environment on the substituent attached to the silica surface. In the present case, the C=O groups are indeed probes for the local environment at the surface through the perturbation suffered by the value of the C=O stretching frequency. To the best of our knowledge, no experimental IR has been detected for the specific quinone functionalized silica case considered here. Therefore, the DFT simulations can provide essential information for interpreting experiments, hopefully carried out in the future.[29]

From the experimental side, the C=O frequency of benzoquinone covalently attached to graphite surfaces was observed at around 1630 cm^{-1}.[52] Moreover, some of us have recently reported experimental IR

spectra of a silica-based network with organic functional groups, where carbonyl frequencies of the quinone groups are found at ≈ 1650 cm^{-1}.[16]

A useful quantity to be compared with the experiment is the shift suffered by the C=O stretching frequency of the quinone at the silica surface in comparison with the value of the free molecule. PBE-D2 values are affected by systematic error due to the adopted functional and basis set quality. Therefore, to bring our computed frequencies on a common scale with the experimental ones, we considered a simplified model for which accurate experiments are available. This will allow to derive a scaling factor bringing the computed Δν(C=O) shift to coincide with the experimental ones. The same scaling factor will then be adopted to scale the shifts computed for the present, more complex, quinone-substituted silica surfaces. The reference system is acetone adsorbed on amorphous silica, recently studied experimentally by Crocellà *et al.*.[53] For the modeling, we used the same silica surface. The resulting, most stable adsorbed state is shown in Figure 6. The acetone molecule engages two relatively short hydrogen bonds with silanols E and H of the surface. In same way, the environment of the C=O group in acetone is similar to that of one C=O group of the quinone in structure C (see Figure 4). The computed adsorption energy ΔE = -93 $kJ \cdot mol^{-1}$ (BSSE corrected[54]) and Δν(CO) = -73 cm^{-1}, should be compared with the experimental values of ΔH = -75 $kJ \cdot mol^{-1}$ and Δν(CO) = -44 cm^{-1} for acetone adsorption on pyrogenic amorphous Aerosil 200 nonporous silica, in which acetone adsorbed in the low pressure regime forms two hydrogen bonds with the silanol groups (see Ref.[53] for more details). The computed ΔE value will become less negative when zero point energy contribution and thermal corrections are taken into account, bringing the agreement with the experimental ΔH value even closer.

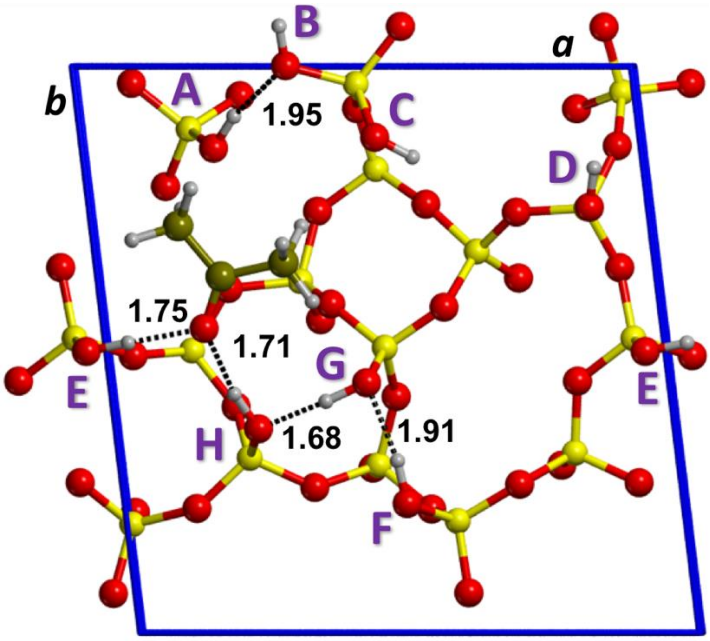

Figure 6. Acetone adsorption on the hydroxylated surface of amorphous silica. Hydrogen bond distances reported in Å. Color code for atoms: silicon in yellow, oxygen in red, hydrogen in light grey, carbon in green.

The computed Δν(CO) shift is overestimated with respect to the experimental value. Two are the reasons for that: i) systematic error in the adopted method, as mentioned before; ii) differences in the hydrogen bond pattern between the model and the real system. Indeed, in our model, the hydrogen bond labelled H in Figure 6 is particularly strong, being the terminal of a chain. This, in turn, will increase the shift suffered by the C=O group. On the contrary, in the experiment, it is claimed that only isolated silanol groups are engaging hydrogen bond with the C=O functionality. To compensate for all above mentioned effects, we define a scaling factor s as:

$$s = \Delta\nu(C{=}O)_{CALC}/\Delta\nu(C{=}O)_{EXPT} = 0.61 \quad (2)$$

and apply it to rescale the shifts computed for the quinone-functionalized surfaces. We are well aware of the limitation of our procedure, as in the quinone group the two C=O groups are involved in a π-resonant electronic system, at variance with the acetone case.

We simulated the IR spectra for B, C and D mono-functionalized models, as well as for the bi-functionalized HE one.

Experimental IR spectrum[55] of the o-benzoquinone molecule gives for the anti-symmetric and symmetric C=O stretching frequencies values of 1690 and 1665 cm^{-1} with an internal shift of 36 cm^{-1}, in good agreement with the shift of 25 cm^{-1} computed at PBE-D2 level for 4-ethyl-ortho-benzoquinone.

Table 2. Computed IR C=O stretching modes (cm^{-1}) for three mono-functionalized models and the bi-functionalized one, compared to the 4-ethyl-o-benzoquinone molecule, with relative shifts. Unscaled and scaled (s-) values by applying the scaling factor s = 0.601, see text for details.

Model	**ν_a(CO)**	**$\Delta\nu_a$(CO)**	**s-$\Delta\nu_a$(CO)**	**ν_s(CO)**	**$\Delta\nu_s$(CO)**	**s-$\Delta\nu_s$(CO)**
4-ethyl-o-benzoquinone (ref.)	1694	-		1658	-	-
Mono-B	1657	-37	-22	1632	-26	-16
Mono-C	1660	-57	-34	1601	-34	-20
Mono-D	1678	-9	-5	1649	-16	-10
Bi-HE	1688, 1671	-23, -16	-14, -10	1642, 1635	-23, -6	-14, -4

The Δ(CO) stretching shifts – both unscaled and scaled, are reported in Table 2 for the considered models, while the corresponding computed spectra in the C=O stretching frequency window, based on unscaled frequencies, are shown in Figure 7.

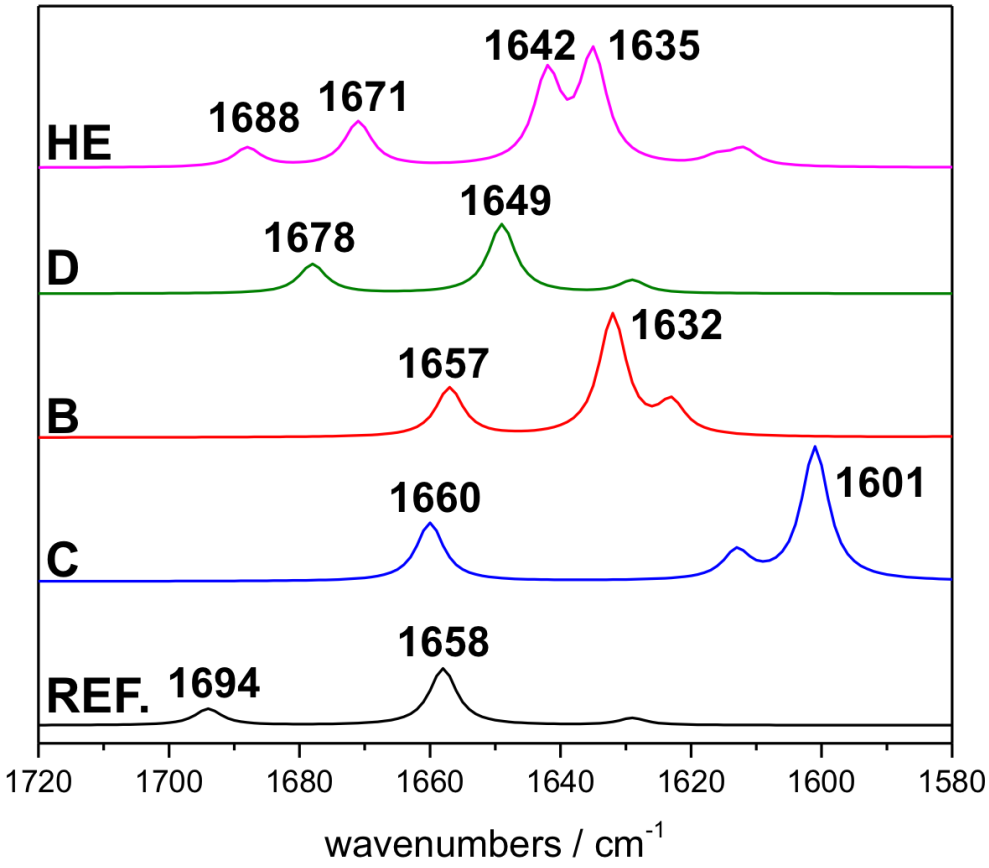

Figure 7. Computed IR spectra in the C=O stretching region for the three mono-functionalized C, B and D models and the bi-functionalized case HE, compared to the reference molecule, 4-ethyl-o-benzoquinone, displayed in Figure 1c).

As expected, the largest bathochromic shifts are computed for the most stable C model (Table 1), due to the formation of two moderately strong hydrogen bonds (1.79 and 1.86 Å) on one CO ($\Delta\nu$(CO)=-34 cm^{-1}) and one strong hydrogen bond (1.76 Å) with the second CO (($\Delta\nu$(CO)=-57 cm^{-1}). For the D case (Figure 7) the associated bathochromic shifts are much lower (($\Delta\nu$(CO)=-9 and -16 cm^{-1}), due to the presence of only one hydrogen bond (1.88 Å). For all cases, the tiny band at 1623 (B), 1613 (C), 1629 (D) and 1612, 1616 (HE) cm^{-1} is associated to the C=C stretching frequency of the quinone ring, which is found at 1629 cm^{-1} in the reference molecule. We think that these data can be used by researchers as a guide in their interpretation of the often crowded IR spectra for similar systems.

AIMD on selected quinone functionalized silica models

Ab initio molecular dynamics (AIMD) simulations were performed with the CP2K code for the most stable mono-functionalized C model. The goal of this investigation was to understand if we were overlooking parts of the PES in our static approach. We carried out an explorative AIMD run of 10 ps at 450K in the NVT ensemble starting from the optimized C-model geometry (Figure 4). The Root Mean Square Deviation (RMSD) along the trajectory for the atomic positions of the quinone functionality (red line, Figure 9), shows the quinone moiety oscillating around the starting position in the first part of the simulation, and then further departing for longer time evolution (average RMSD: 1.24 Å, maximum RMSD: 2.50 Å).

We were interested in the changes of hydrogen bond distances with time to see if they were stable during the dynamics, with the purpose to find any other stable configuration of the quinone functionalization on the silica surface. Figure 8 reports this analysis, focusing on the four hydrogen bonds established among quinone oxygen atoms, labelled O1 and O2, and the four silanols (A, D, E and H, see Figures 1b and c for labelling). The most interesting observation is the formation of a new hydrogen bond between O1 and A silanol after 6.6 ps of time evolution (as shown by the dramatic drop of the A···O1 distance in the corresponding graph of Figure 8. Obviously, hydrogen bonds E···O1 and H···O1 are correspondingly lost, as shown by peaks in their graphs of Figure 8. The formation of the new hydrogen bond is due to the rotation of the quinone-functionalizing group, and corresponds to a peak in the RMSD labelled as point C' in Figure 9.

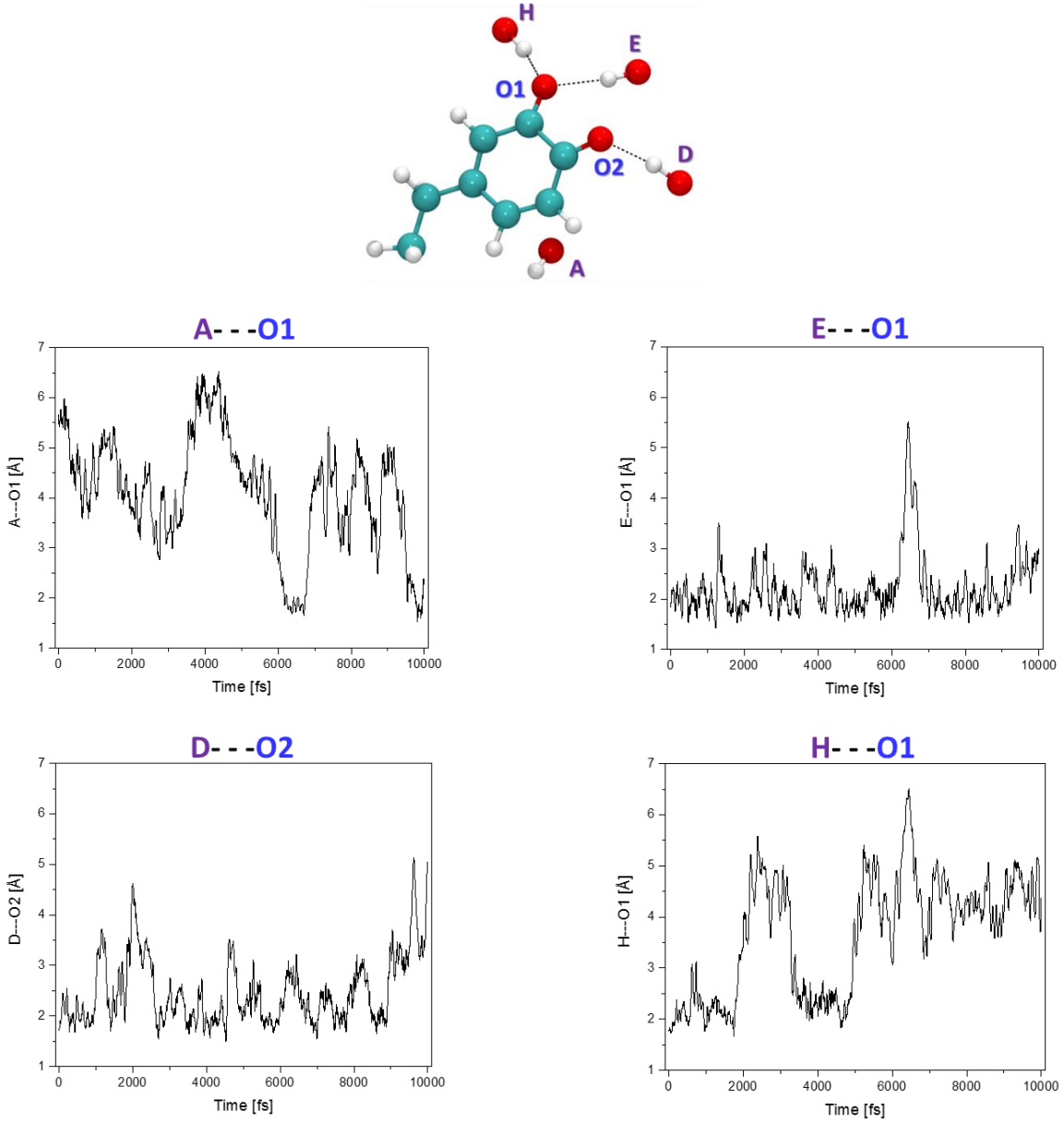

Figure 8. Hydrogen bond length values established among the CO groups of the functionalization and different surface silanols during the AIMD simulation for the case of C-functionalized silica. First row: local view of the geometry of interaction, labelling the two different oxygen 1 and 2; second and third rows: hydrogen bond length variation with respect to the simulation time for each of the four hydrogen bonds of O1 and O2 with silanols A, D, E and H. Color code for atoms: oxygen in red, hydrogen in white, carbon in cyan.

We fully optimized the structure extracted from the MD after 6.6 ps with the static PBE-D2 method. The resulting ΔE (see equation (1)), for this new C' case, while still negative (ΔE = -4.5 kJ mol^{-1}) is higher by about 11 kJ·$mol^{-1}$with respect to the original C case. Figure 9 b) illustrates the top view of the optimized C' model, where one C=O is part of a hydrogen bond chain with silanols A and B, forming a

stabilizing ring-like structure with the Si-C bond of the functionalization.

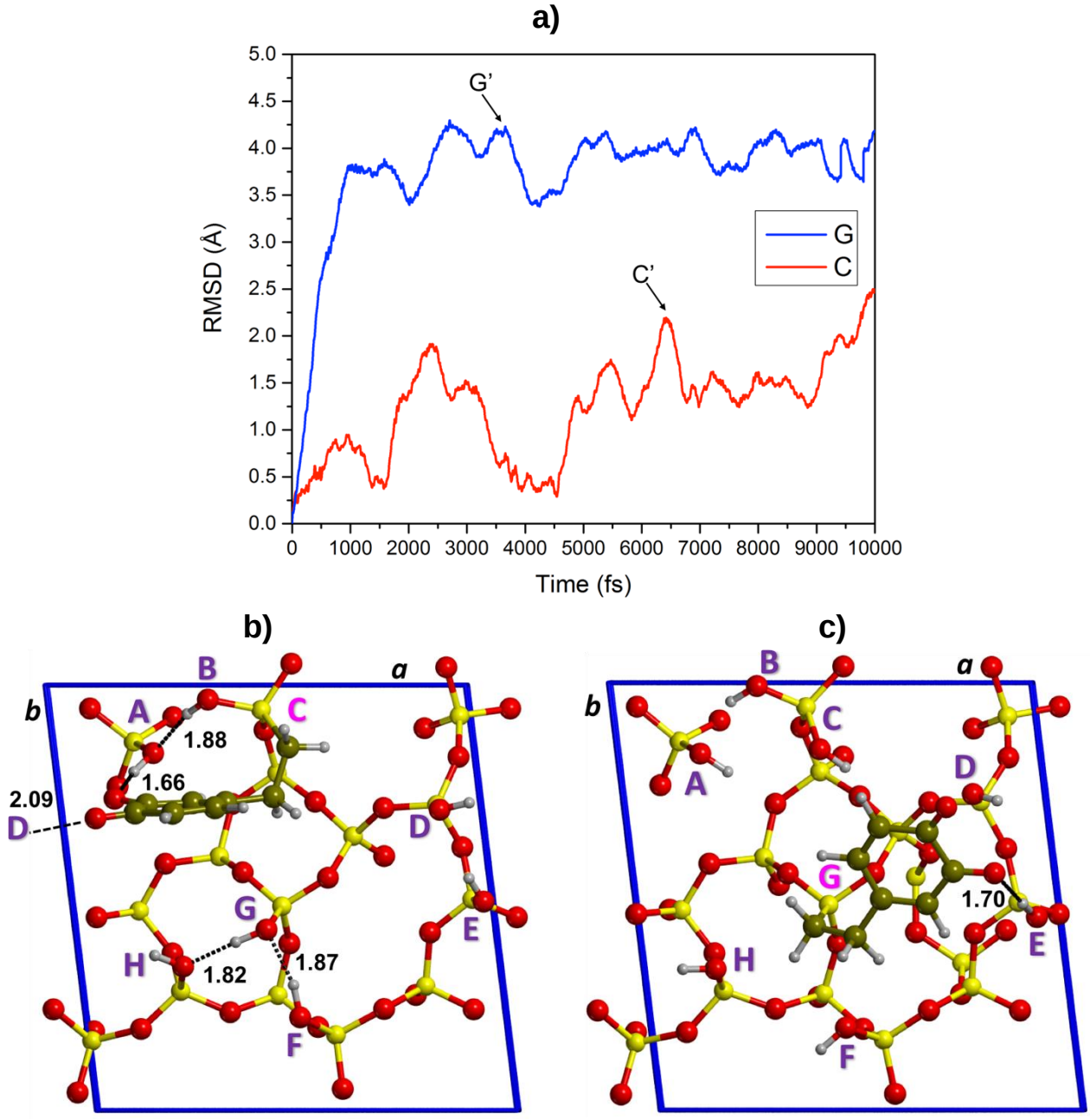

Figure 9. a) Root Mean Square Deviations (RMSD) along the AIMD trajectories for the atomic positions of the quinone functionality, in the G and C cases; corresponding b) C' and c) G' optimized structures. Color code for atoms: silicon in yellow, oxygen in red, hydrogen in light grey, carbon in green.

The G model (least stable) was also simulated at 450 K to see if the added kinetic term was able to let it evolve in a more stable configuration. Indeed, as shown by the RMSD profile of Figure 9a), in less than 2 ps the system shifted from the initial structure to a new geometry, that was then mostly retained until

the end of the trajectory (average RMSD: 3.74 Å, maximum RMSD: 4.30 Å). This suggests that the original configuration, albeit a local minimum in the potential energy surface, is separated by very low barriers from other more stable configurations, in which it transforms very quickly, therefore being probably scarcely representative of the real system. The origin of the instability is the lack of contact between the quinone moiety and the silica surface (minimum dispersion contribution). The new G' structure (extracted at time = 3.6 ps, in the RMSD of Figure 9a) has been optimized with the static approach and is reported in Figure 9 c). The quinone moiety is now flat with respect to the surface, as in the C case, and forms one hydrogen bond with a surface silanol. The ΔE with respect to equation (1) is 71 kJ·mol^{-1} instead of 109 (Table 1), gaining about 38 kJ·mol^{-1} in stability with respect to the original model. *Ab initio* molecular dynamics is therefore revealed as a crucial tool to complement static DFT simulations.

Schiff base formation on the quinone functionalized silica surfaces

We took the optimum mono-functionalized models to further react with the NH_2 group of allylamine ($CH_2CHCH_2NH_2$), as a model of basic functionality present in potential antimicrobial peptides. Figure 10 reports the general scheme of the Schiff base formation, known to proceed via a Ping Pong mechanism.[56] The corresponding reaction is written in equation (3), showing the formation of an imine compound as reaction product.

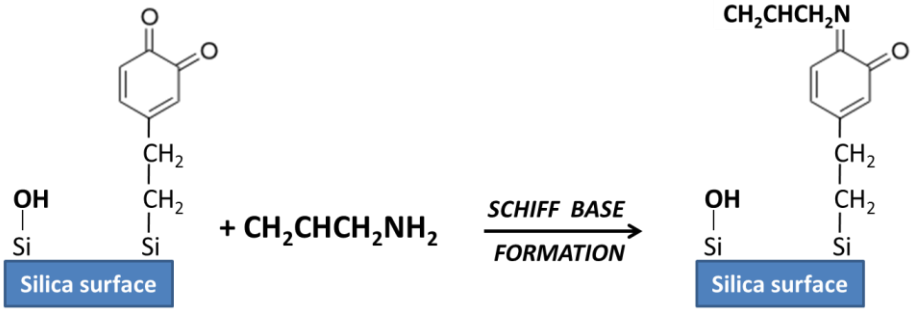

Figure 10. Scheme of the covalent bonding between a quinone functionalized silica surface and allylamine according to a Schiff base formation.

$$Silica(OH)_7(CH_2CH_2\text{-quinone}) + CH_2CHCH_2NH_2 \rightarrow Silica(OH)_7(CH_2CH_2\text{-imine}) + H_2O \quad (3)$$

As for equation (1), also in this case the reaction is hypothetical and only serves to compare the reaction energy of different functionalized models. The reaction energy values (ΔE) are reported in Table 3 for all the simulated models (see Figure 1a for the labelling). For sake of brevity, we reported in Figure 11 the optimized structures of the four models B, D, E and H for which we also computed the vibrational ν(CO) and ν(CN) features. Figure ESI2 in the Electronic supplementary information file shows the complete set of all seven models.

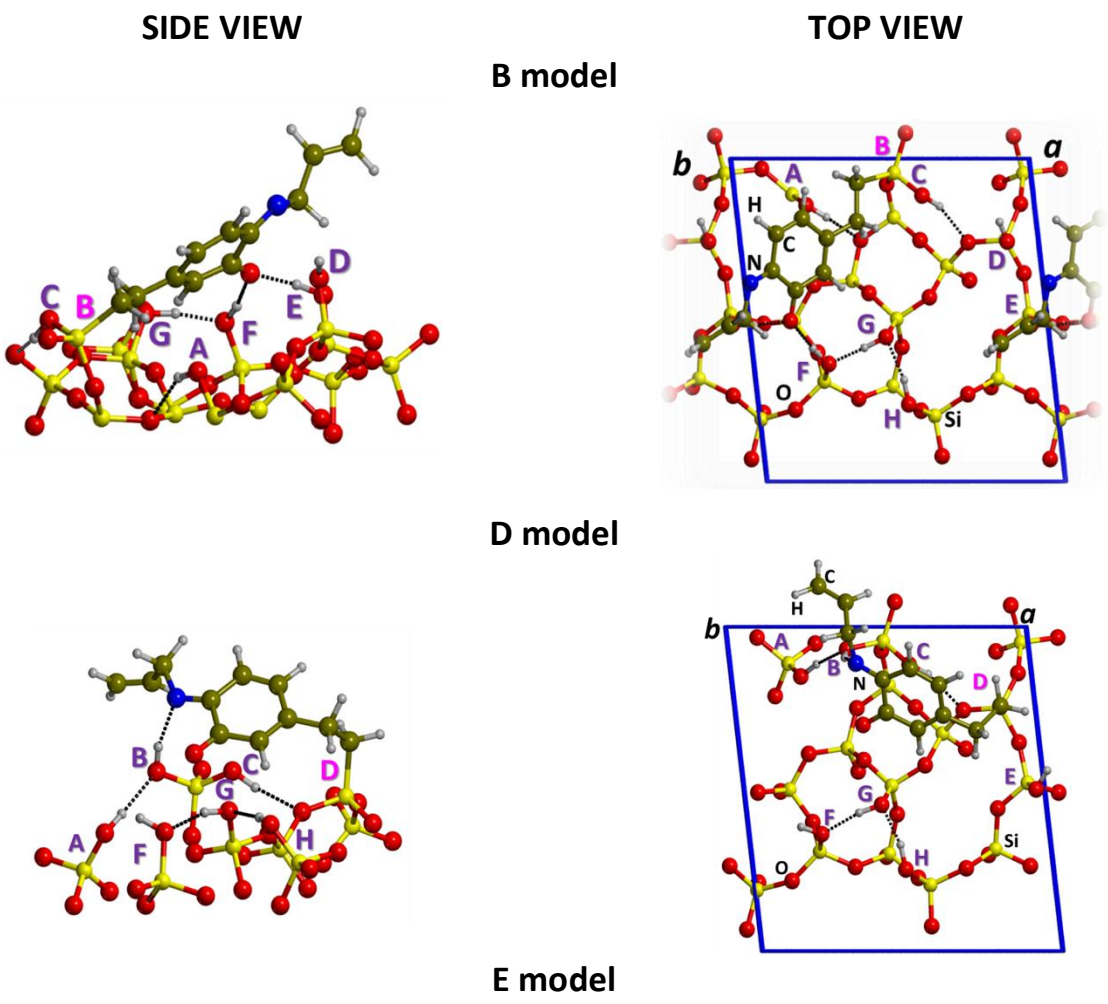

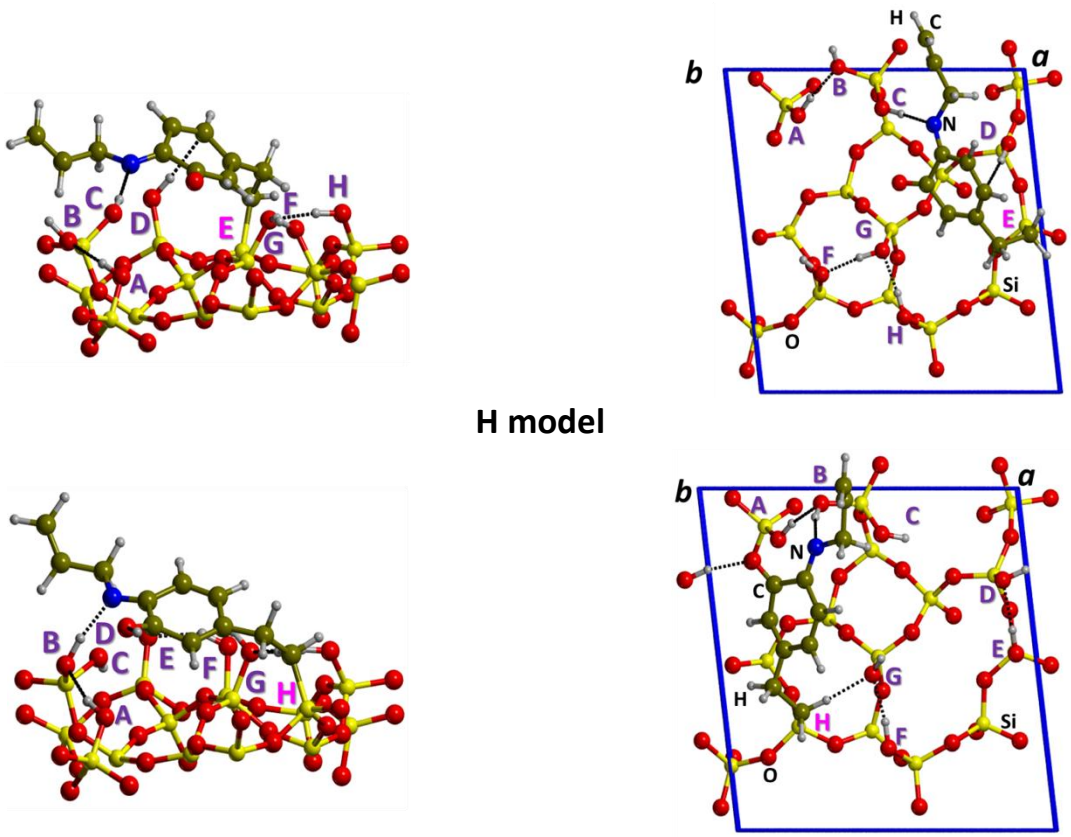

Figure 11. Side (left) and top (right) view of the imine products (see eq. 3) starting from different mono-functionalized models, i.e. B, D, E and H. Color code for atoms: silicon in yellow, oxygen in red, hydrogen in light grey, carbon in green, nitrogen in blue. Unit cell borders in blue, hydrogen bonds as black dotted lines; functionalized silanol labelled in pink.

From data of Table 3, the H-mono-functionalized model is the most stable one, due to the presence of a H···N bond with the B silanol (1.75 Å) and of the H···O=C bond with the D one (1.85 Å). Moreover, this model is characterized by a good balance among the electronic and dispersive contributions to the energy. The stability order is H > E > F > B > D > C > G models. Structures E, F (see Figure ESI2) and D contain hydrogen bonds between the immino nitrogen atom with surface silanol. As for the mono-functionalized model described in the previous section, structure G is the least stable one, as no contact of the immine group is made with the surface (structure shown in Figure ESI2). Interestingly, data of Table 3 shows that the Schiff formation reaction energies are completely uncorrelated with the relative stability of the quinone-functionalized models (see Table 2). This means that the Schiff reaction greatly changes the PES of the system, therefore stabilities obtained for the quinone-functionalization cannot be used as

estimator for the energies of further steps in the functionalization process. As for the latter cases, the Schiff reaction energy is entirely driven by maximizing both the hydrogen bonds with the C=O group and dispersive interactions with the silica surface.

Table 3. Computed reaction energy values (ΔE), IR CO (unscaled/scaled for the scaling factor already applied in Table 2) and CN stretching modes and corresponding shifts with respect to the free imine molecule (cm^{-1}) for all the Schiff base formation product models obtained by the mono-functionalized cases, labelled from B to H according to the substituted silanol, as in Figure 1a) and b). All energy values expressed in $kJ \cdot mol^{-1}$, while frequencies in cm^{-1}.

n=1 - MONO							
	B	**C**	**D**	**E**	**F**	**G**	**H**
ΔE	-24.1	-4.2	-21.7	-28.2	-27.3	-0.6	-33.5
ΔΔE	9.4	29.4	11.9	5.3	6.3	33.0	0.0
ΔE_E	-23.3	6.9	6.4	4.2	4.9	8.3	-13.5
ΔE_D	-0.8	-11.1	-28.1	-32.5	-32.2	-8.9	-20.0
ν(CO), Δν(CO)/scaled	1496, -167/-100	-	1661, -2/-1	1676, 13/8	-	-	1626, -37/-22
ν(CN), Δν(CN)	1565, -8	-	1565, -8	1570, -3	-	-	1568, -5

For all models shown in Figure 11 we computed the IR spectra, and Table 3 reports the ν(CO) and ν(CN) frequency of the imine moiety and the corresponding shifts with respect to the reference molecule (the same molecule of Figure 1c with one O substituted by the CH_2CHCH_2N moiety) in the gas phase. Generally speaking, the ν(CN) is almost unaffected by the interaction with the silica surface, with very small bathochromic shifts (maximum of 8 cm^{-1}). In the B model the C=O group establishes two hydrogen bonds with two silanols, resembling the structural motif already commented in the mono-functionalized C model and for the reference acetone molecule adsorbed at surface. Indeed, the CO stretching of this B model suffer a large bathochromic shift of about 167 cm^{-1} (100 cm^{-1} after scaling). Interestingly, for the E model, an hypsochromic shift resulted, since no CO group is involved in hydrogen bond with the surface. Also in the D case, no hydrogen bond is established and the ν(CO) resulted almost unperturbed. As for the quinone-functionalization, these data can guide analysis of measured IR spectra, aiming at correlating experimental data to the atomistic details of the interactions.

Conclusions

In the present paper, we have modeled at PBE-D2 the surface functionalization of a model of amorphous silica by means of 4-ethyl-ortho-benzoquinone groups, which become chemically attached trough the silanol groups. We have studied all possible substitution to each available SiOH group, by manually docking the substituent to exploit the maximum number of hydrogen bonds with the remaining silanol groups. By considering a hypothetical reference surface chemical reaction, we established an energy ranking of each substituted model. Two key points emerged as essential for the stability of the substituted model: i) the hydrogen bond strength between the CO groups and the surface silanols and ii) the dispersive interaction of the whole quinone with the silica surface. We did not detect other specific interactions. The above points are important from the methodological point of view, as computational methods not including dispersive correction to the DFT energy are prone to fail badly in the modelling of adsorption of large molecules on oxide surfaces. The adoption of *ab initio* molecular dynamics to explore the potential energy surface revealed the bounty of our manual docking, but also possible flaws for high-energy structures, which are unstable when temperature effects are included. The functionalized silica is the starting point for linking potential antimicrobial peptide by nucleophilic attack the C=O functionalities through peptide basic NH_2 groups. We simulate this process by reacting the allylamine $CH_2CHCH_2NH_2$ via Schiff reaction with the quinone functionalized models. An important methodological result is that the Schiff formation reaction energies are completely uncorrelated with the relative stability of the quinone-functionalized models. As for the quinone-functionalized cases, the reaction energy is entirely driven by the ability of the functionalizing moiety to establish both hydrogen bonds with the C=O group and dispersive interactions with the silica surface.

The present simulation also predicted infrared features in the C=O stretching region, which is visible in the experimentally functionalized materials.[17] When CO behaves as hydrogen bond acceptor, the ν(CO) resulted bathochromically-shifted, with scaled values less than 20 cm^{-1} for quinone-functionalized

models, but up to 100 cm^{-1} for the Schiff reacted functionalized groups. For the latter cases, the CN stretching is only moderately affected, suffering bathchromic shifts less than 10 cm^{-1}. Calculations are already ongoing in our laboratory to analyze other reaction mechanisms, such as Michael addition, and the adoption of lysine and cysteine as better models of antimicrobial peptide functionality compared to allylamine.

Acknowledgements

This research was carried out in the framework of the European ERA.NET METABIO project "innovative METhod to elaborate bio-inspired stable Antibacterial surface on metallic BIOmaterials for dental implants" funded by the Luxembourgish agency "Fonds National de la Recherche" (INTER/MERA/888845). The vast majority of the calculations was carried out on the FERMI HPC facility of the CINECA Supercomputing Center, located in Bologna, Italy, thanks to the ISCRA (Italian SuperComputing Resource Allocation) class B project SIL4SKIN.

Footnote

† Electronic supplementary information (ESI) available: computational details (static calculations and amorphous silica surface coordinates); complete computed IR spectra for models B, C, D and HE; side and top views of the imine products as obtained by the different mono-functionalized models, from B to H.

4. References

(1) Besinis, A.; De Peralta, T.; Tredwin, C. J.; Handy, R. D. Review of Nanomaterials in Dentistry: Interactions with the Oral Microenvironment, Clinical Applications, Hazards, and Benefits. *ACS Nano* **2015**, *9* (3), 2255–2289.

(2) Gristina, A. G. Biomaterial-Centered Infection: Microbial Adhesion versus Tissue Integration.

Science **1987**, *237* (4822), 1588–1595.

(3) Subbiahdoss, G.; Kuijer, R.; Grijpma, D. W.; van der Mei, H. C.; Busscher, H. J. Microbial Biofilm Growth vs. Tissue Integration: "The Race for the Surface" Experimentally Studied. *Acta Biomater.* **2009**, *5* (5), 1399–1404.

(4) Zasloff, M. Antimicrobial Peptides of Multicellular Organisms. *Nature* **2002**, *415* (6870), 389–395.

(5) Ding, Y.; Wang, W.; Fan, M.; Tong, Z.; Kuang, R.; Jiang, W.; Ni, L. Antimicrobial and Anti-Biofilm Effect of Bac8c on Major Bacteria Associated with Dental Caries and Streptococcus Mutans Biofilms. *Peptides* **2014**, *52*, 61–67.

(6) Martinez Rodriguez, N. R.; Das, S.; Kaufman, Y.; Wei, W.; Israelachvili, J. N.; Waite, J. H. Mussel Adhesive Protein Provides Cohesive Matrix for Collagen Type-1α. *Biomaterials* **2015**, *51*, 51–57.

(7) Dalsin, J. L.; Hu, B. H.; Lee, B. P.; Messersmith, P. B. Mussel Adhesive Protein Mimetic Polymers for the Preparation of Nonfouling Surfaces. *J. Am. Chem. Soc.* **2003**, *125* (14), 4253–4258.

(8) Wei, W.; Yu, J.; Gebbie, M. a.; Tan, Y.; Martinez Rodriguez, N. R.; Israelachvili, J. N.; Waite, J. H. Bridging Adhesion of Mussel-Inspired Peptides: Role of Charge, Chain Length, and Surface Type. *Langmuir* **2015**, *31* (3), 1105–1112.

(9) Faure, E.; Falentin-Daudré, C.; Jérôme, C.; Lyskawa, J.; Fournier, D.; Woisel, P.; Detrembleur, C. Catechols as Versatile Platforms in Polymer Chemistry. *Prog. Polym. Sci.* **2013**, *38* (1), 236–270.

(10) Sedó, J.; Saiz-Poseu, J.; Busqué, F.; Ruiz-Molina, D. Catechol-Based Biomimetic Functional Materials. *Adv. Mater.* **2013**, *25* (5), 653–701.

(11) Lee, S.-B.; González-Cabezas, C.; Kim, K.-M.; Kim, K.-N.; Kuroda, K. Catechol-Functionalized Synthetic Polymer as a Dental Adhesive to Contaminated Dentin Surface for a Composite Restoration. *Biomacromolecules* **2015**, *16* (8), 2265–2275.

(12) Manakhov, A.; Moreno-Couranjou, M.; Choquet, P.; Boscher, N. D.; Pireaux, J. J. Diene Functionalisation of Atmospheric Plasma Copolymer Thin Films. *Surf. Coatings Technol.* **2011**, *205* (SUPPL. 2).

(13) Duday, D.; Vreuls, C.; Moreno, M.; Frache, G.; Boscher, N. D.; Zocchi, G.; Archambeau, C.; Van De Weerdt, C.; Martial, J.; Choquet, P. Atmospheric Pressure Plasma Modified Surfaces for Immobilization of Antimicrobial Nisin Peptides. *Surf. Coatings Technol.* **2013**, *218* (1), 152–161.

(14) Mauchauffé, R.; Moreno-Couranjou, M.; Boscher, N. D.; Van De Weerdt, C.; Duwez, A.-S.; Choquet, P.; Mauchauffe, R.; Moreno-Couranjou, M.; Boscher, N. D.; Weerdt, C. Van De; et al. Robust Bio-Inspired Antibacterial Surfaces Based on the Covalent Binding of Peptides on Functional Atmospheric Plasma Thin Films. *J. Mater. Chem. B* **2014**, *2* (32), 5168–5177.

(15) Wang, G.; Loh, G. C.; Pandey, R.; Karna, S. P. Novel Two-Dimensional Silica Monolayers with Tetrahedral and Octahedral Configurations. *J. Phys. Chem. C* **2015**, *119* (27), 15654–15660.

(16) Mauchauffé, R.; Bonot, S.; Moreno-Couranjou, M.; Detrembleur, C.; Boscher, N. D.; Van De Weerdt, C.; Duwez, A. S.; Choquet, P. Fast Atmospheric Plasma Deposition of Bio-Inspired Catechol/Quinone-Rich Nanolayers to Immobilize NDM-1 Enzymes for Water Treatment. *Adv. Mater. Interfaces* **2016**, *3* (8), 1500520.

(17) Mauchauffé, R.; Moreno-Couranjou, M.; Boscher, N. D.; Duwez, A. S.; Choquet, P. Liquid-

Assisted Plasma-Enhanced Chemical Vapor Deposition of Catechol and Quinone-Functionalized Coatings: Insights into the Surface Chemistry and Morphology. *Plasma Process. Polym.* **2016**, *13* (8), 843–856.

(18) Heinz, H.; Ramezani-Dakhel, H.; Sanchez, C.; Belleville, P.; Popall, M.; Nicole, L.; Osada, M.; Sasaki, T.; Scrivener, K. L.; Nonat, A.; et al. Simulations of Inorganic–bioorganic Interfaces to Discover New Materials: Insights, Comparisons to Experiment, Challenges, and Opportunities. *Chem. Soc. Rev.* **2016**, *45* (2), 412–448.

(19) Meißner, R. H.; Schneider, J.; Schiffels, P.; Colombi Ciacchi, L. Computational Prediction of Circular Dichroism Spectra and Quantification of Helicity Loss upon Peptide Adsorption on Silica. *Langmuir* **2014**, *30* (12), 3487–3494.

(20) Lutz, H.; Jaeger, V.; Berger, R.; Bonn, M.; Pfaendtner, J.; Weidner, T. Biomimetic Growth of Ultrathin Silica Sheets Using Artificial Amphiphilic Peptides. *Adv. Mater. Interfaces* **2015**, *2* (17), 1500282.

(21) Butenuth, A.; Moras, G.; Schneider, J.; Koleini, M.; Köppen, S.; Meißner, R.; Wright, L. B.; Walsh, T. R.; Ciacchi, L. C. Ab Initio Derived Force-Field Parameters for Molecular Dynamics Simulations of Deprotonated Amorphous-SiO 2/water Interfaces. *Phys. Status Solidi Basic Res.* **2012**, *249* (2), 292–305.

(22) Cirac, A. D.; Moiset, G.; Mika, J. T.; Koçer, A.; Salvador, P.; Poolman, B.; Marrink, S. J.; Sengupta, D. The Molecular Basis for Antimicrobial Activity of Pore-Forming Cyclic Peptides. *Biophys. J.* **2011**, *100* (10), 2422–2431.

(23) Kristoffersen, H. H.; Shea, J.-E.; Metiu, H. Catechol and HCl Adsorption on TiO2 (110) in Vacuum and at the Water–TiO2 Interface. *J. Phys. Chem. Lett.* **2015**, *2* (110), 2277–2281.

(24) Mian, S. A.; Gao, X.; Nagase, S.; Jang, J. Adsorption of Catechol on a Wet Silica Surface: Density Functional Theory Study. *Theor. Chem. Acc.* **2011**, *130* (2), 333–339.

(25) Mian, S. A.; Yang, L.-M.; Saha, L. C.; Ahmed, E.; Ajmal, M.; Ganz, E. A Fundamental Understanding of Catechol and Water Adsorption on a Hydrophilic Silica Surface: Exploring the Underwater Adhesion Mechanism of Mussels on an Atomic Scale. *Langmuir* **2014**, *30* (23), 6906–6914.

(26) Sinnecker, S.; Flores, M.; Lubitz, W. Protein-Cofactor Interactions in Bacterial Reaction Centers from Rhodobacter Sphaeroides R-26: Effect of Hydrogen Bonding on the Electronic and Geometric Structure of the Primary Quinone. A Density Functional Theory Study. *Phys. Chem. Chem. Phys.* **2006**, *8* (48), 5659–5670.

(27) Yeh, I.-C.; Lenhart, J. L.; Rinderspacher, B. C. Molecular Dynamics Simulations of Adsorption of Catechol and Related Phenolic Compounds to Alumina Surfaces. *J. Phys. Chem. C* **2015**, *119* (14), 7721–7731.

(28) Saiz-Poseu, J.; Alcón, I.; Alibés, R.; Busqué, F.; Faraudo, J.; Ruiz-Molina, D. Self-Assembly of Alkylcatechols on HOPG Investigated by Scanning Tunneling Microscopy and Molecular Dynamics Simulations. *CrystEngComm* **2012**, *14* (1), 264–271.

(29) Corno, M.; Delle Piane, M.; Monti, S.; Moreno-Couranjou, M.; Choquet, P.; Ugliengo, P.; Piane, M. D.; Monti, S.; Moreno-Couranjou, M.; Choquet, P.; et al. Computational Study of Acidic and Basic Functionalized Crystalline Silica Surfaces as a Model for Biomaterial Interfaces. *Langmuir* **2015**, *31* (23), 6321–6331.

(30) Perdew, J. P.; Burke, K.; Ernzerhof, M.; of Physics, D.; Quantum Theory Group Tulane

University, N. O. L. 70118 J. Generalized Gradient Approximation Made Simple. *Phys. Rev. Lett.* **1996**, *77* (18), 3865–3868.

(31) Grimme, S. Semiempirical GGA-Type Density Functional Constructed with a Long-Range Dispersion Correction. *J. Comput. Chem.* **2006**, *27* (15), 1787–1799.

(32) Dovesi, R.; Orlando, R.; Erba, A.; Zicovich-Wilson, C. M.; Civalleri, B.; Casassa, S.; Maschio, L.; Ferrabone, M.; De La Pierre, M.; D'Arco, P.; et al. CRYSTAL14 : A Program for the Ab Initio Investigation of Crystalline Solids. *Int. J. Quantum Chem.* **2014**, *114*, 1287−1317.

(33) Nada, R.; Nicholas, J. B.; McCarthy, M. I.; Hess, A. C. Basis Sets for Ab Initio Periodic Hartree-Fock Studies of Zeolite/Adsorbate Interactions: He, Ne, and Ar in Silica Sodalite. *Int. J. Quantum Chem.* **1996**, *60*, 809–820.

(34) Schäfer, A.; Horn, H.; Ahlrichs, R. Fully Optimized Contracted Gaussian Basis Sets for Atoms: Li to Kr. *J. Chem. Phys.* **1992**, *97*, 2571.

(35) Ugliengo, P.; Viterbo, D.; Chiari, G. MOLDRAW: Molecular Graphics on a Personal Computer. *Z. Krist.* **1993**, *208* (Part-2), 383.

(36) Pascale, F.; Zicovich-Wilson, C. M.; López Gejo, F.; Civalleri, B.; Orlando, R.; Dovesi, R. The Calculation of the Vibrational Frequencies of Crystalline Compounds and Its Implementation in the CRYSTAL Code. *J. Comput. Chem.* **2004**, *25* (6), 888–897.

(37) Zicovich-Wilson, C. M.; Pascale, F.; Roetti, C.; Saunders, V. R.; Orlando, R.; Dovesi, R. Calculation of the Vibration Frequencies of ?-Quartz: The Effect of Hamiltonian and Basis Set. *J. Comput. Chem.* **2004**, *25* (15), 1873–1881.

(38) Noel, Y.; Zicovich-Wilson, C. M.; Civalleri, B.; D'Arco, P.; Dovesi, R. Polarization Properties of ZnO and BeO: An Ab Initio Study through the Berry Phase and Wannier Functions Approaches. *Phys. Rev. B* **2001**, *65* (1), 14111.

(39) Orlando, R.; Piane, M.; Bush, I. J.; Ugliengo, P.; Ferrabone, M.; Dovesi, R.; Delle Piane, M.; Bush, I. J.; Ugliengo, P.; Ferrabone, M.; et al. A New Massively Parallel Version of CRYSTAL for Large Systems on High Performance Computing Architectures. *J. Comput. Chem.* **2012**, *33* (28), 2276–2284.

(40) Hutter, J.; Iannuzzi, M.; Schiffmann, F.; VandeVondele, J. cp2k: Atomistic Simulations of Condensed Matter Systems. *Wiley Interdiscip. Rev. Comput. Mol. Sci.* **2014**, *4* (1), 15–25.

(41) VandeVondele, J.; Krack, M.; Mohamed, F.; Parrinello, M.; Chassaing, T.; Hutter, J. Quickstep: Fast and Accurate Density Functional Calculations Using a Mixed Gaussian and Plane Waves Approach. *Comput. Phys. Commun.* **2005**, *167*, 103–128.

(42) Goedecker, S.; Teter, M.; Hutter, J. Separable Dual-Space Gaussian Pseudopotentials. *Phys. Rev. B* **1996**, *54* (3), 1703–1710.

(43) VandeVondele, J.; Hutter, J. Gaussian Basis Sets for Accurate Calculations on Molecular Systems in Gas and Condensed Phases. *J. Chem. Phys.* **2007**, *127* (11), 114105.

(44) Bussi, G.; Donadio, D.; Parrinello, M. Canonical Sampling through Velocity Rescaling. *J. Chem. Phys.* **2007**, *126* (1), 1–7.

(45) Delle Piane, M.; Corno, M.; Ugliengo, P. Does Dispersion Dominate over H-Bonds in Drug–Surface Interactions? The Case of Silica-Based Materials As Excipients and Drug-Delivery Agents. *J. Chem. Theory Comput.* **2013**, *9* (5), 2404–2415.

(46) Delle Piane, M.; Vaccari, S.; Corno, M.; Ugliengo, P. Silica-Based Materials as Drug Adsorbents:

First Principle Investigation on the Role of Water Microsolvation on Ibuprofen Adsorption. *J. Phys. Chem. A* **2014**, *118* (31), 5801–5807.

(47) Gignone, A.; Delle Piane, M.; Corno, M.; Ugliengo, P.; Onida, B. Simulation and Experiment Reveal a Complex Scenario for the Adsorption of an Antifungal Drug in Ordered Mesoporous Silica. *J. Phys. Chem. C* **2015**, *119* (23), 13068–13079.

(48) Zhuravlev, L. T. Concentration of Hydroxyl-Groups on the Surface of Amorphous Silica. *Langmuir* **1987**, *3* (3), 316–318.

(49) Delle Piane, M.; Corno, M.; Pedone, A.; Dovesi, R.; Ugliengo, P. Large-Scale B3LYP Simulations of Ibuprofen Adsorbed in MCM-41 Mesoporous Silica as Drug Delivery System. *J. Phys. Chem. C* **2014**, *118* (46), 26737–26749.

(50) Rimola, A.; Costa, D.; Sodupe, M.; Lambert, J.-F.; Ugliengo, P. Silica Surface Features and Their Role in the Adsorption of Biomolecules: Computational Modeling and Experiments. *Chem. Rev.* **2013**, *113*, 4216–4313.

(51) Musso, F.; Casassa, S.; Corno, M.; Ugliengo, P. How Strong Are H-Bonds at the Fully Hydroxylated Silica Surfaces? Insights from the B3LYP Electron Density Topological Analysis. *Struct. Chem.* **2017**, 1–7, DOI: 10.1007/s11224-016-0906-7.

(52) Ramesh, P.; Sampath, S. Electrochemical and Spectroscopic Characterization of Quinone Functionalized Exfoliated Graphite. *Analyst* **2001**, *126* (11), 1872–1877.

(53) Crocellà, V.; Cerrato, G.; Magnacca, G.; Morterra, C. Adsorption of Acetone on Nonporous and Mesoporous Silica. *J. Phys. Chem. C* **2009**, *113* (37), 16517–16529.

(54) Boys, S. F.; Bernardi, F. The Calculations of Small Molecular Interaction by the Difference of Separate Total Energies. Some Procedures with Reduced Error. *Mol. Phys.* **1970**, *19*, 553–566.

(55) Kashima, C.; Tomotake, A.; Omote, Y. Photolysis of the Ozonide Derived from 1,4-Benzodioxins. Synthesis of Labile O-Benzoquinone. *J. Org. Chem.* **1987**, *2* (8), 5616–5621.

(56) Davidson, V. L.; Graichen, M. E.; Jones, L. H. Mechanism of Reaction of Allylamine with the Quinoprotein Methylamine Dehydrogenase. *Biochem. J.* **1995**, *308*, 487–492.

Toc Graphics

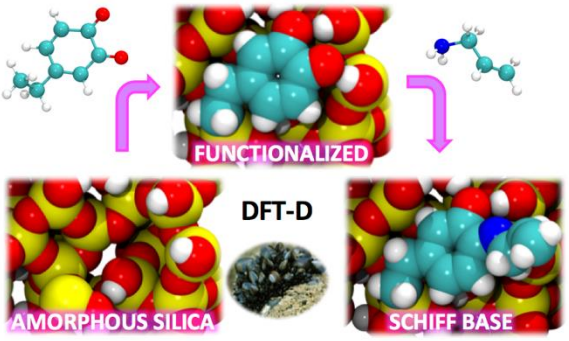

Structural and IR features of amorphous silica surfaces, functionalized by ortho-benzoquinone groups, were computed for a deeper knowledge of multifunctional coatings with antimicrobial properties.